Eur. Phys. J. Plus (2026) 141:1043
https://doi.org/10.1140/epjp/s13360-026-08213-3

THE EUROPEAN PHYSICAL JOURNAL PLUS

Regular Article

Laser wakefield acceleration in nanostructured plasmas

Alexandre Bonatto[1,a], **Bruno Silveira Nunes**[2,b], **Jon Imanol Apiñaniz-Aginako**[3], **Laura Bandiera**[4], **Cristian Bontoiu**[5], **Gianluca Cavoto**[6,7], **Illya Drebot**[8], **Giancarlo Gatti**[3], **Jorge Giner-Navarro**[9], **Bifeng Lei**[5,10], **Pablo Martín-Luna**[11], **Ilaria Rago**[6], **Juan Rodríguez-Pérez**[9], **Alexei Sytov**[4], **Pablo Cirrone**[12], **Mirko Salomón Alva-Sánchez**[1], **Ricardo Elgul Samad**[2], **Nilson Dias Vieira Jr.**[2], **Constantinos Valagiannopoulos**[13], **Carsten Peter Welsch**[5,10], **Guoxing Xia**[10,14], **Jiaqi Zhang**[10,14], **Javier Resta-López**[9,15,c]

[1] Graduate Program in Information Technology and Healthcare Management, and the Beam Physics Group, Federal University of Health Sciences of Porto Alegre, Porto Alegre, RS 90050-170, Brazil
[2] Nuclear and Energy Research Institute, IPEN-CNEN, São Paulo, SP CEP 05508-000, Brazil
[3] Centro de Láseres Pulsados, Bulding M5, Science Park, Calle Adaja 8, 37185 Villamayor, Salamanca, Spain
[4] INFN Sezione di Ferrara, Via Saragat 1, 44122 Ferrara, Italy
[5] Department of Physics, University of Liverpool, Oxford Street, Liverpool L69 7ZE, UK
[6] Dipartimento di Fisica, Sapienza Università di Roma, Piazzale Aldo Moro 2, 00185 Roma, Italy
[7] INFN Sezione di Roma, Piazzale Aldo Moro 2, 00185 Roma, Italy
[8] INFN Sezione di Milano, Via G. Celoria 16, 20133 Milano, Italy
[9] Instituto de Ciencia de los Materiales (ICMUV), Universidad de Valencia, 46980 Paterna, Spain
[10] Cockcroft Institute, Keckwick Lane, Daresbury, Warrington WA4 4AD, UK
[11] Instituto de Física Corpuscular (IFIC), Universidad de Valencia - CSIC, 46980 Paterna, Spain
[12] INFN Sezione di Catania, Via Santa Sofia 64, 95123 Catania, Italy
[13] School of Electrical and Computer Engineering, National Technical University of Athens, 15773 Zografou, Greece
[14] Department of Physics and Astronomy, University of Manchester, Oxford Road, Manchester M13 9PL, UK
[15] Departamento de Física Aplicada y Electromagnetismo, Universidad de Valencia, 46100 Burjassot, Spain

Received: 27 February 2026 / Accepted: 17 August 2026

Abstract Solid-state plasma wakefield acceleration has recently attracted attention as a novel method for achieving unprecedented ultrahigh acceleration gradients on the order of 1 TeV/m or beyond. In this context, recent advancements in nanofabrication techniques have opened up the possibility of creating structured plasmas with tailored properties. For instance, the utilization of carbon nanotube (CNT) bundles holds great potential for generating stable plasmas with electron densities reaching as high as 10^{22} cm^{-3}, i.e., orders of magnitude higher than conventional gaseous plasmas. As part of a new collaborative effort called NanoAc, we have conducted particle-in-cell (PIC) simulations to investigate laser wakefield acceleration in nanostructured solid-state plasmas based on CNT arrays. Our results confirm the attainment of wakefields at the TV/m scale. Additionally, we observed self-injection, sub-femtosecond bunch formation, and electron acceleration in micrometer-scale targets, yielding kinetic energies on the order of a few tens of MeV. These findings open up promising possibilities to design novel ultracompact accelerators and radiation sources. In this paper, we report recent simulation results from the NanoAc collaboration and describe ongoing efforts toward future experimental tests at available laser facilities.

1 Introduction

Over the past decades, plasma-based acceleration in gaseous media has evolved from a theoretical concept into a mature experimental field. Accelerating gradients on the GeV/m scale, long anticipated [1, 2], are now routinely achieved at many laboratories around the world [3–8]. These advances have established plasma accelerators as strong candidates for compact next-generation machines, with prospective applications ranging from medicine [9] and industry [10] to high-energy physics [11].

Since the achievable accelerating gradient scales with plasma density, increasing the density offers a direct path toward higher fields. This consideration has motivated the exploration of solid-state plasmas, formed via ionization, whose densities (10^{22}–10^{24}

[a] e-mail: abonatto@ufcspa.edu.br (corresponding author)
[b] e-mail: brunosnunes@usp.br (corresponding author)
[c] e-mail: javier2.resta@uv.es (corresponding author)

Published online: 11 September 2026

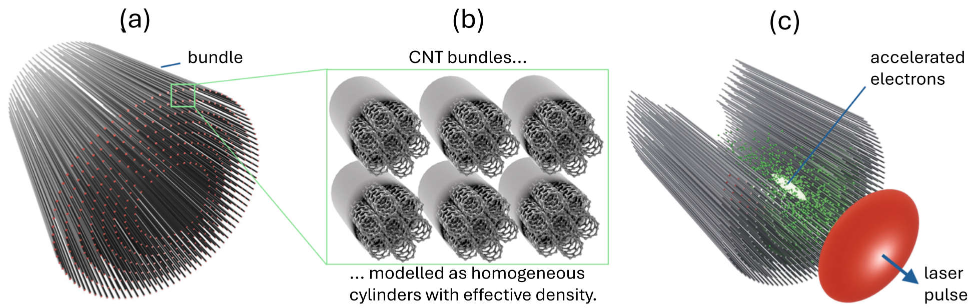

Fig. 1 **a** Schematic of a target based on CNT aligned bundles, with a circular aperture to allow the transmission of laser pulses through it. **b** Zoomed-in view of the cross-sectional perspective of CNT bundles. **c** Schematic view of the microtube accelerator concept. A driving laser pulse propagates axially through the target, ionizing the structure and exciting wakefields that self-inject and accelerate electrons from the structure itself

cm^{-3}) exceed those of gaseous plasmas by several orders of magnitude. In principle, such densities could support accelerating gradients in the TeV/m range, representing a substantial step beyond current capabilities.

Wakefield acceleration in solid-state plasmas was proposed decades ago for crystal channels [12, 13], with predicted gradients of 1–10 TeV/m, and was later extended to nanotubes driven by X-ray pulses [14, 15]. These schemes, however, depend on ultrashort X-ray drivers that are not yet routinely available, and natural crystal channels impose angstrom-scale acceptance constraints. In contrast, nanostructured targets, with tunable channels orders of magnitude wider, may offer a path to overcome both limitations.

In interactions involving intense femtosecond laser pulses and solid targets, experiments have shown that nanostructuring the target surface enhances the emission of hot electrons (~ 100 keV – 1 MeV) [16–18] as well as X-ray radiation [19–23]. This enhancement arises from the direct laser acceleration of ionized electrons within the nanochannels. Additionally, it has been experimentally demonstrated that nanostructured targets improve laser-driven ion acceleration through the target normal sheath acceleration (TNSA) mechanism [24]. However, these processes do not involve resonant laser wakefield acceleration (LWFA).

A microtube accelerator concept based on resonant LWFA has been recently proposed in [25–27]. It is composed of porous or nanowire structures made of CNT arrays as indicated in Fig. 1. Because of their exceptional optoelectronic, thermal, and mechanical properties, CNT-based materials represent highly promising candidates for the fabrication of the proposed targets. In particular, CNT-based structures are attracting increasing interest within the accelerator physics community [28, 29]. In addition, planar configurations such as multilayer graphene have also been explored as potential media for particle acceleration [30].

In contrast to earlier numerical studies [15], which proposed LWFA in metallic crystals driven by exawatt-class X-ray pulses, we demonstrate that resonant LWFA can be achieved using an 800 nm infrared laser operating at the terawatt scale. This significantly reduces the technological constraints for implementation at existing facilities, enabling the generation of TeV/m accelerating gradients without reliance on attosecond X-ray lasers and thereby expanding the experimental and application landscape.

Based on this novel microtube accelerator concept composed of CNT bundles, different acceleration regimes have been explored depending on the laser and geometric parameters, as well as on the type of driver—either a high-density charged particle beam or a high-power laser [31, 32]. More recently, numerical studies have demonstrated that the proposed microtube accelerator concept also has the potential to operate as a coherent synchrotron radiation (CSR) emitter [33].

To investigate the feasibility, performance, and potential applications of the microaccelerator concept presented here, we have established the NanoAc collaboration [34–36]. In this manuscript, we report full 3D PIC simulations results that build upon the previous NanoAc study in Ref. [27], and we outline ongoing efforts toward the design of a proof-of-principle experiment.

2 Simulation results

The simulations were performed using the open-source PIC code WarpX [37], in full 3D Cartesian geometry. The domain was set to $-3.5 \le z \le 27.5\,\mu\mathrm{m}$ longitudinally and $-3.5\,\mu\mathrm{m} \le x,\ y \le 3.5\,\mu\mathrm{m}$ transversely, with $N_{x,y,z} = 1024$ grid cells in each direction, and the number of macroparticles per cell, $N_{\mathrm{PPC}} = 8\ (2 \times 2 \times 2)$. Open boundary conditions were used for particles and electromagnetic fields in all directions. The laser had circular polarization, normalized strength $a_0 = 21.6$, wavelength $\lambda_0 = 800\,\mathrm{nm}$, waist $w_0 = 1.5\,\mu\mathrm{m}$, pulse duration $\tau = 2.67\,\mathrm{fs}$ (FWHM), peak intensity $I_0 = 10^{21}\ \mathrm{W/cm^2}$, peak power of $\sim 35.3\,\mathrm{TW}$, and pulse energy $E = 100\,\mathrm{mJ}$.

Figure 2 shows the cross section of a target composed of CNT bundles (red dots), modeled as solid carbon cylinders with radius $r_b = 12.5\,\mathrm{nm}$ and density $n_b = 10^{22}\ \mathrm{cm}^{-3}$. Here, n_b denotes the bundle-averaged carbon density assigned to each homogeneous CNT-bundle cylinder, rather than the atomic density of an ideal CNT wall or of compact graphitic carbon. This coarse-grained value accounts phenomenologically for the internal structure of realistic CNT bundles, including voids, inter-tube packing, CNT radii, number of walls, and filling fraction. While neither this approach nor conventional PIC algorithms can model the microscopic solid-state effects of actual CNT materials, both frameworks effectively capture the collective plasma response of the nanostructured medium [26].

The bundles are distributed along concentric cylindrical shells (gray lines), which serve as theoretical (immaterial) guides for the spatial arrangement. The distribution is designed such that each shell maintains a constant effective density: For a given shell,

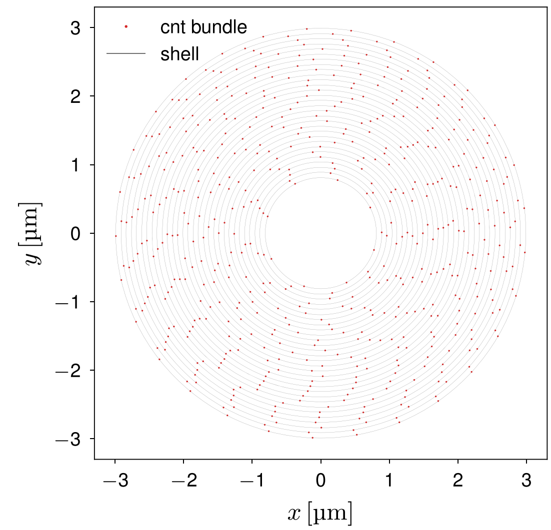

Fig. 2 Transverse cross section of the CNT target composed of 548 CNT bundles (red points) distributed over 30 concentric shells (gray lines). Each shell has a thickness of 25 nm, corresponding to CNTs with a radius of 12.5 nm, and adjacent shells are separated by a 50 nm gap. This configuration results in an effective target density of approximately 10^{20} cm^{-3}. The target features a central hollow region with inner radius $R_{in} = 0.8$ μm and an outer radius of $R_{\text{out}} = 3$ μm

the number of bundles and their angular spacing were calculated to ensure uniform effective density along the shell circumference, with bundle positions determined by a random initial phase angle for each shell. This shell-by-shell construction provides a second averaging step, yielding a target with overall effective density $n_{\text{eff}} \simeq 10^{20}$ cm^{-3}, which is the relevant quantity for laser propagation and wakefield excitation. The target features a central aperture with inner radius $R_{in} = 0.8$ μm, which facilitates propagation of the laser core through the target.

This target configuration reproduces the geometry of Ref. [27], with the simulations performed here using higher spatial resolution and particles per cell than in the referenced work. Despite representing the same physical system, different postprocessing approaches prevent direct comparison of the results. In the previous work, the beam was characterized using particles trapped within the wakefield bubble volume, whereas here the beam is defined from all particles exiting the target with forward momentum corresponding to kinetic energies above 20 MeV. While this approach may yield beam quality metrics lower than those reported previously, it provides a more experimentally relevant characterization of the beam, since it relies on particles selected according to an energy threshold rather than on particles identified through their confinement within an idealized wakefield structure.

Figure 3 presents the simulation results. Following the mechanism described in Ref. [27], the laser pulse ionizes the CNT bundles and drives electrons toward the outer shells, generating a propagating wakefield bubble similar to those observed in conventional laser wakefield acceleration with gaseous plasma targets. Electrons are self-injected at the rear of the bubble, where they experience longitudinal electric fields on the order of TV/m. Panels (a–f) show snapshots of the laser–target interaction. A wakefield bubble approximately 4.5 μm wide propagates through the target. The left column (a, c, e) displays the electron density n_e/n_0 surrounding the bubble (blue colormap), while the right column (b, d, f) shows the longitudinal electric field E_z (blue–white–red colormap). The accelerated electrons forming the extracted bunch, defined as electrons exiting the target with kinetic energies above 20 MeV at the final time step, are identified a posteriori and backtracked throughout the simulation. The selected charge of this bunch is called Q_{sel}. This procedure ensures that the same electrons are followed over time, avoiding changes in bunch composition that would arise from selecting particles based on their instantaneous energies. These electrons are rendered with a yellow–green colormap indicating their energies. Light-gray horizontal lines show a subset of the CNT bundles, allowing for a schematic visualization of the target geometry.

Panels (a, b) capture the early propagation stage at $z \simeq 4$μm, where a well-defined wakefield bubble has formed with self-injection occurring at its rear. The longitudinal electric field within the wake exceeds 10 TV/m at this stage. Panels (c, d) show the bubble near the target center, where trapped electrons continue gaining energy, forming a reasonably collimated bunch with the most energetic particles reaching $\sim$ 40 MeV. Panels (e, f) show the bunch after exiting the target. Despite undergoing deceleration due to positive longitudinal electric fields beyond the target boundary, as shown in panel (f), the bunch contains electrons with energies approaching 60 MeV.

Panels (g–i) present phase-space projections of the extracted bunch using a white–yellow–red–black density colormap. Panels (g) and (h) show the transverse phase spaces (x–x' and y–y'), revealing beam divergence (RMS) of $\sim$ 0.08 rad and displacement from the target axis, consistent with betatron oscillations. Panel (i) shows the longitudinal phase space (z–E_k), where the bunch extends approximately 1 μm longitudinally. Panel (j) presents the energy spectrum, spanning from 20 MeV (the selection threshold) to nearly 60 MeV, with a mean energy of 38.7 MeV, energy spread (RMS) of 9.3 MeV, and selected charge of 493 pC. Despite the substantial energy spread, a well-defined quasi-monoenergetic peak is observed, centered at 45.4 MeV with FWHM spread of $\sim$ 12 MeV, containing approximately 50% of the total bunch charge. For the target length of 15 μm, the mean and quasi-monoenergetic peak energies correspond to average acceleration gradients of 2.6 TeV/m and 3.0 TeV/m, respectively.

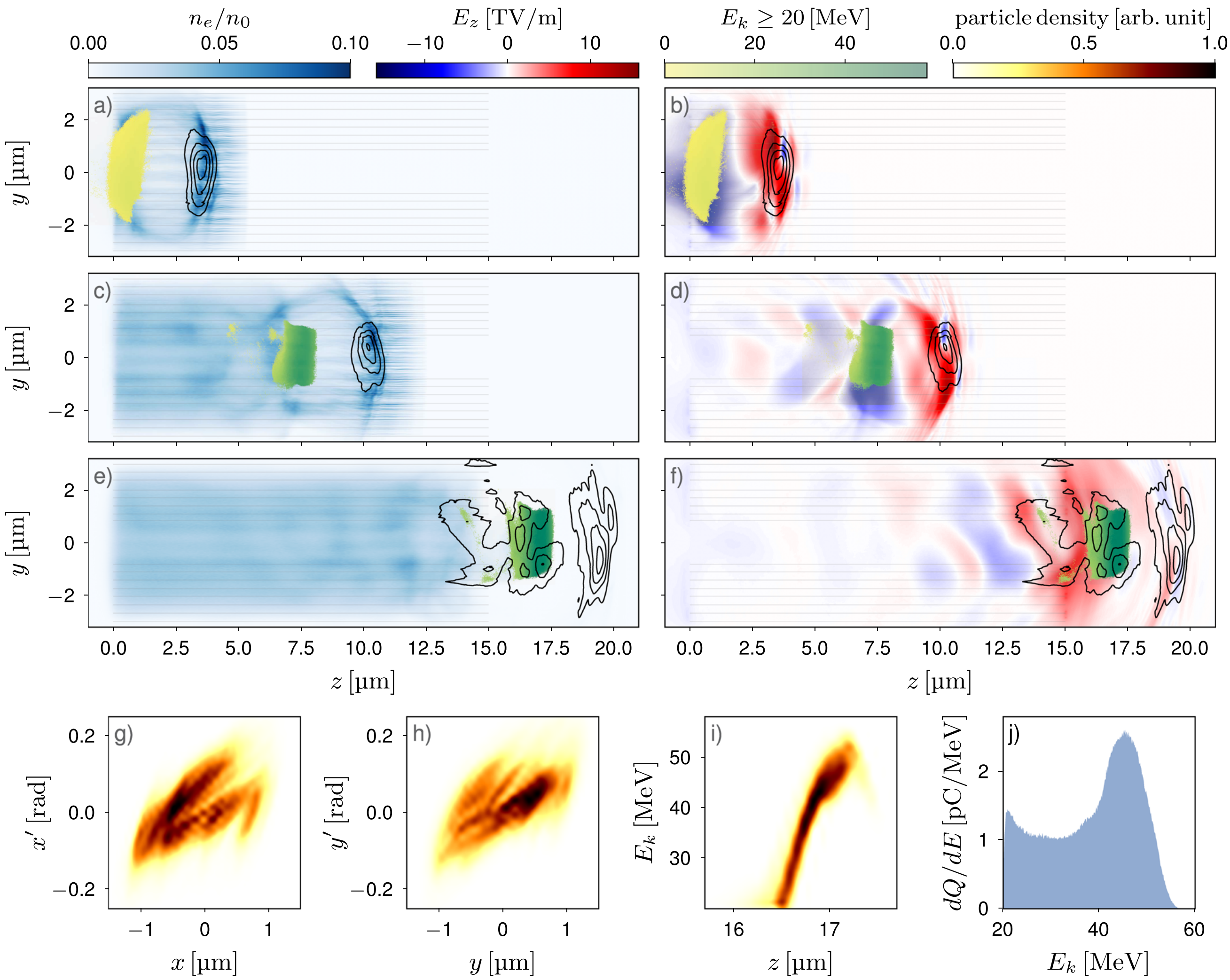

Fig. 3 Electron density (blue colormap), longitudinal electric field (blue–white–red colormap), and energy of the accelerated electrons (yellow–green colormap) for a CNT-based target with an effective electron density of $n_e \simeq 10^{20}$ cm^{-3}. Closed black contour lines indicate iso-intensity contours of the laser pulse envelope, with intensity increasing toward the innermost contour. Panels **a**–**f** correspond to three snapshots taken at successive times during the simulation: Panels **a**, **c**, and **e** show the electron density distribution, while panels **b**, **d**, and **f** show the corresponding longitudinal electric field. The light-gray horizontal lines represent a subset of the CNT bundles and are included solely to provide a schematic visualization of the target geometry. Panels **g**–**i** present the transverse and longitudinal phase spaces of the extracted electron bunch, where $x' = u_x/u_z$ and $y' = u_y/u_z$; the white–yellow–red–black colormap indicates the normalized particle density. Panel (j) shows the energy spectrum of the accelerated beam

Fig. 4 Electron energy spectra obtained from three independent simulations with different random seeds used to generate the initial phase angle distribution of the shells

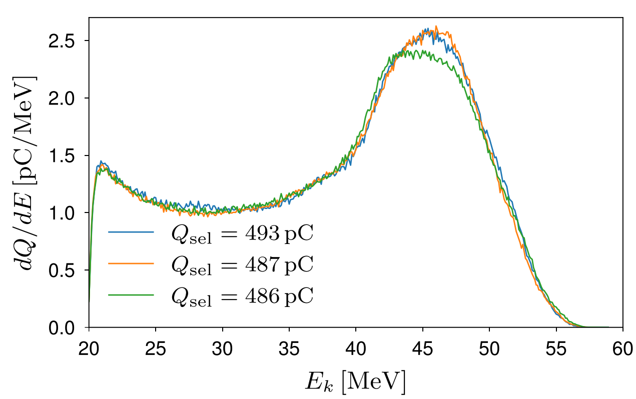

To assess the sensitivity of the results to the bundle distribution within the target, two additional simulations were performed using different random seeds for the initial phase angles of the shells. Figure 4 compares the electron energy spectra obtained from

Table 1 Electron bunch parameters at extraction

Parameter	Value (avg. ± std. dev.)	Unit	Description
Q_{sel}	489 ± 4	pC	Charge
$\bar{E}_k$	38.7 ± 0.1	MeV	Average kinetic energy
σ_{E_k}	9.3 ± 0.1	MeV	Kinetic energy spread (RMS)
$\bar{A}$	2.58 ± 0.01	TeV/m	Avg. accel. gradient
η	18.9 ± 0.2	%	Energy conv. eff.
Δz	0.71 ± 0.01	µm	Bunch length (FWHM)
Δx	1.7 ± 0.1	µm	Horizontal size (FWHM)
Δy	1.7 ± 0.2	µm	Vertical size (FWHM)
$\epsilon_{n,x}$	2.5 ± 0.1	µmrad	Norm. emittance (RMS)
$\epsilon_{n,y}$	2.5 ± 0.1	µmrad	Norm. emittance (RMS)
Θ_x	77 ± 2	mrad	Divergence (RMS)
Θ_y	77 ± 1	mrad	Divergence (RMS)

the three simulations (including the case shown in Fig. 3). Despite the different bundle arrangements, the spectra are very similar: all extend from the 20 MeV selection threshold to nearly 60 MeV and exhibit a well-defined quasi-monoenergetic peak centered at approximately 45 MeV, with the selected charge varying by only 7 pC among the three cases. Table 1 summarizes the beam parameters, reported as averages over the three target realizations; the reference run shown in Fig. 3 carries 493 pC, close to the three-run average of 489 ± 4 pC.

It is instructive to place these results in the context of previous solid-density acceleration concepts. Crystal-channel wakefield accelerators [12, 13] and X-ray-driven nanotube schemes [14] predict accelerating gradients of 1–10 TeV/m, but depend on ultrashort X-ray drivers that remain unavailable. Optical-driver studies in carbon nanostructures reported a ∼4.8 TeV/m accelerating gradient and 6.9 MeV average kinetic energy over 1.5 µm using an ultraviolet (100 nm wavelength) laser pulse in multilayer graphene [30], and 27.9 MeV average kinetic energy with 867 pC over 15 µm using an infrared (800 nm wavelength) laser pulse in CNT-bundle targets [27]. Beam-driven schemes in CNT channels predict even higher gradients, up to hundreds of TeV/m [31, 38, 39], but require near-solid-density electron beams expected only from future facility upgrades. The results presented here are consistent with these scalings while relying exclusively on terawatt-class, 800 nm wavelength laser technology available at existing facilities. Moreover, since the accelerated bunch is characterized from all electrons exiting the target rather than from particles selected within the wakefield structure, the reported beam parameters provide a realistic quantitative reference for the proof-of-principle experiment under development within the NanoAc collaboration.

The normalized transverse emittances of the extracted bunch, $\epsilon_{n,x} = \epsilon_{n,y} = 2.5 \pm 0.1$ µm rad (Table 1), reflect the relatively large RMS divergence of $\sim$ 77 mrad at extraction. Combined with a peak current of several tens of kA—a consequence of nearly half a nanocoulomb concentrated in a sub-micrometer bunch—these values correspond to a normalized 5D brightness $B_{n,5\text{D}} = 2I/(\epsilon_{n,x}\epsilon_{n,y}) \gtrsim 10^{16}$ A m^{-2} rad^{-2}, comparable to values reported for plasma-based sources and indicating that the proposed scheme operates within reach of the high-brightness regime, even before dedicated optimization of the target and laser parameters.

3 Experimental design

The NanoAc collaboration is planning to perform a series of experimental tests on laser-CNT target interactions, to demonstrate TV/m accelerating field in the laboratory and the generation of high-brightness electron beams.

A tentative experimental layout design is illustrated in Fig. 5, where the target samples are mounted on a movable "revolver" type holder within the main experimental chamber. This design enables rapid target renewal and facilitates comparative testing of various target configurations. Their geometries (overall size, length, hollow radius, etc.), material densities, and substrates will be systematically varied and characterized both before and after laser exposure. High-resolution scanning electron microscopy (SEM) will be employed to assess geometry, density uniformity, defects, and postirradiation damage.

The electron beam energy spectrum can be determined using a high-resolution energy spectrometer, based on a dipole magnet in combination with a tungsten pinhole serving as a pencil-beam selector. Electron beam emittance measurements will be enabled through implementation of the pepper-pot technique [40]. This method allows energy resolved transverse emittance measurement. The electron bunch charge will be measured using an integrating current transformer (ICT) [41].

The betatron radiation generated during the interaction will be characterized both spatially and spectrally using an X-ray charge-coupled device (CCD), operated with and without a stacked filter assembly. The intrinsic spatial coherence of the betatron source will be characterized through measurements of its source size, determined using the knife-edge technique [42].

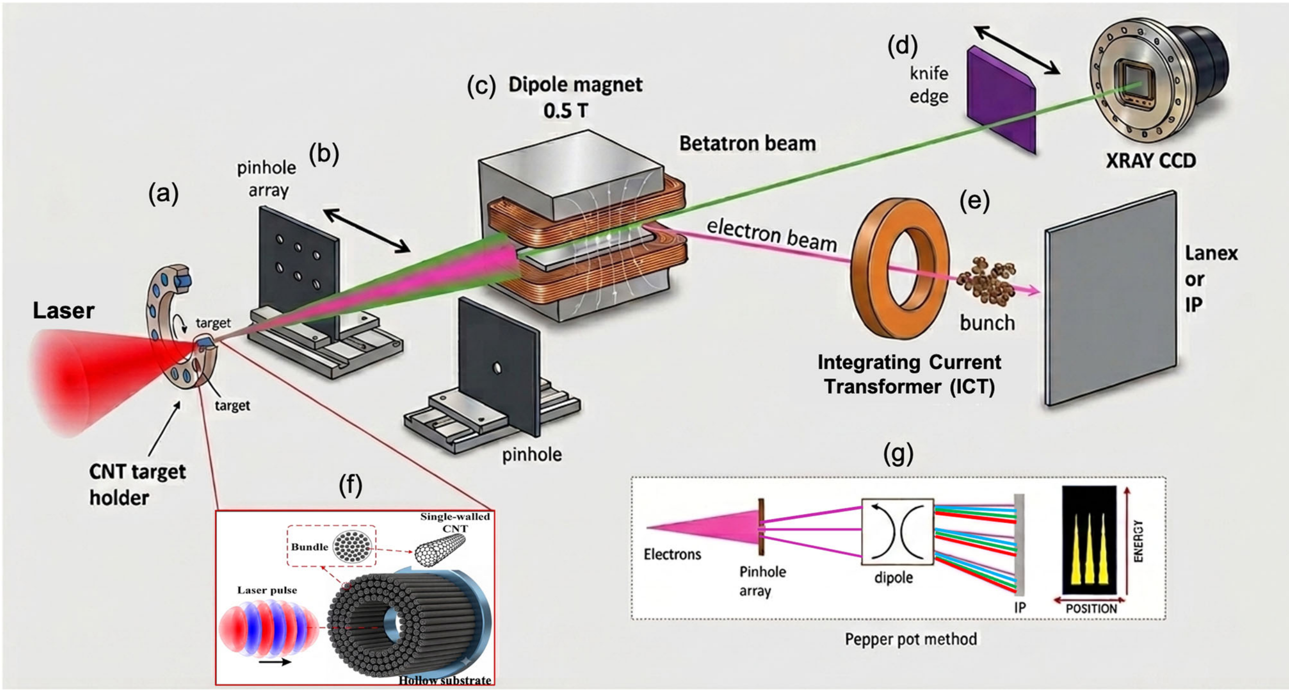

Fig. 5 Schematic of a possible experimental setup: **a** target positioning/refresh strategy, based on a rotary holder; **b** single pinhole or pinhole array for switching between simple electron energy measurement and pepper-pot emittance measurement; **c** dipole magnet for electron separation from betatron axis and electron energy and charge measurement; **d** X-ray CCD for betatron radiation characterization, and knife-edge for source size measurement; **e** integrating current transformer (ICT) for electron bunch charge measurement, and a Lanex or image plate (IP) screen to record the spatially resolved electron distribution, from which the energy spectrum is reconstructed; **f** zoomed view of a nanowired target consisting of CNT bundles; and **g** schematic detail of the pepper-pot method for transverse emittance reconstruction

The fabrication of nanostructured targets is an essential part of the experiment. Modern nanofabrication techniques provide great flexibility in constructing targets based on vertically aligned carbon nanotube (VA-CNT) forests, allowing high precision and tailored geometric characteristics [43–48]. The realization of VA-CNT-based targets and their microscopic and spectroscopic analyses will be performed in specialized facilities at the institutions of collaboration partners, such as the Technology Innovation Through Advanced Nanostructures (TITAN) Laboratory within the Sapienza University of Rome and INFN-Roma, see Fig. 6 [49].

The transition from simulation to experiment involves several practical challenges. Efficient coupling of the laser pulse into the nanostructure relies on the central aperture of the target, imposing micrometer-level tolerances on focusing, alignment, and pointing stability, which will require the implementation of suitable laser–target alignment strategies; in addition, a high temporal-contrast laser pulse is required to prevent premature expansion of the nanostructure by prepulses or amplified spontaneous emission. Regarding target integrity, previous analyses indicate that the displacement of carbon ions remains on the nanometer scale during the femtosecond timescale of the interaction [27, 30], so that the accelerated bunch exits the target before the ion lattice is significantly perturbed; the target nevertheless undergoes destruction on longer timescales, and therefore, the experiment foresees expendable targets, with systematic SEM characterization before and after irradiation. Concerning ionization dynamics, PIC codes treat carbon atoms as independent, neglecting solid-state effects such as covalent bonding; however, at the considered intensities field ionization proceeds rapidly at the leading edge of the pulse, and the ionization energy of carbon in the CNT lattice differs only modestly from the atomic case, so this approximation is not expected to alter the collective dynamics. Finally, since the wakefield excitation is governed by the effective plasma density rather than by the exact positions of individual bundles [26], the scheme is expected to be robust against fabrication imperfections, with the uniformity and reproducibility of the VA-CNT targets to be quantified through the metrology campaign described above.

The required laser parameters, although challenging, could technically be achievable at existing laser facilities. For example, the Center of Pulsed Lasers (CLPU) in Salamanca, Spain, hosts the ultraintense and ultrashort VEGA laser, a Ti:Sapphire CPA-based femtosecond system with three synchronized branches: VEGA-1 (20 TW, 10 Hz), VEGA-2 (200 TW, 10 Hz), and VEGA-3 (1 PW, 1 Hz), all delivering 30 fs pulses [50]. Postcompression and laser pulse characterization will be performed to meet the required specifications. Alignment strategies, which account for intrinsic jitter and precision tolerances, will be developed to ensure reliable laser–target interaction.

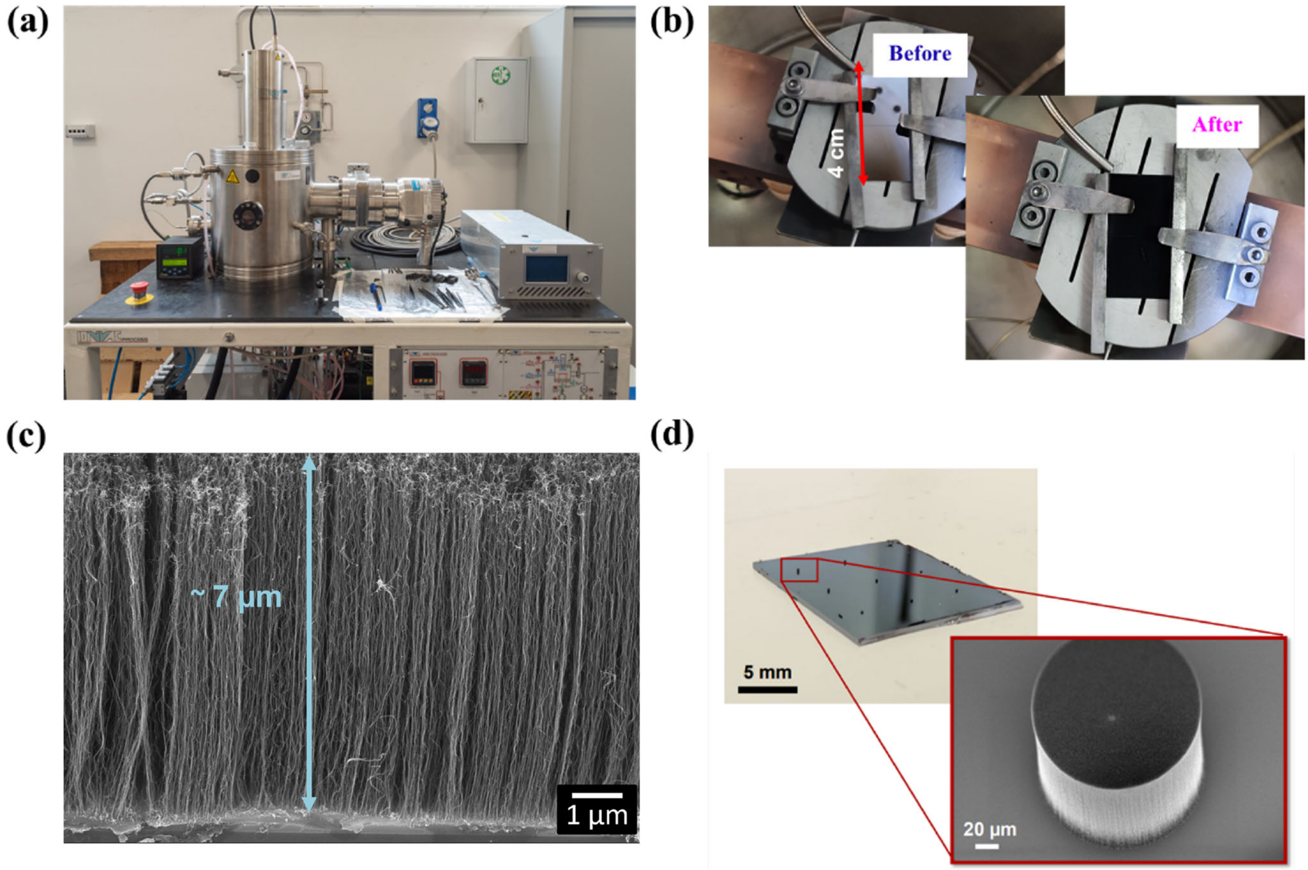

Fig. 6 **a** The TITAN INFN-Sapienza facility at Sapienza University of Rome; **b** silicon substrate mounted on the heating element inside the CVD chamber before (left) and after (right) VA-CNTs synthesis; **c** SEM image of a typical VA-CNT array growth; **d** micropatterned VA-CNTs

4 Conclusions

Building upon our previous studies [27], we have demonstrated here, through full 3D PIC simulations, that LWFA in CNT-based microtube targets can be driven by a TW-level 800 nm wavelength laser pulse, yielding accelerating gradients of several TeV/m and the formation of sub-femtosecond electron bunches with a quasi-monoenergetic peak centered at 45.4 MeV over a target length of approximately 15 μm.

These results substantially relax the technological requirements compared with earlier solid-density LWFA concepts relying on exawatt-class X-ray drivers, while preserving the prospect of ultrahigh gradients enabled by near-solid plasma densities. Notably, this configuration is not an optimized design, but a representative case selected from a preliminary parameter scan for its promising acceleration performance. The systematic dependence on key physical parameters, such as effective density, channel aperture radius, CNT-bundle radius, and laser parameters, remains the subject of an ongoing Bayesian optimization study aimed at maximizing beam quality, charge, energy, and laser-to-beam conversion efficiency. Together with this optimization campaign, ongoing target fabrication efforts within the NanoAc collaboration, and the development of a proof-of-principle experiment, this work establishes a realistic pathway toward the experimental validation of solid-state LWFA in nanostructured media.

Beyond the generation of multi-tens-of-MeV electron beams with substantial charge ($\sim$ 100 pC), the proposed concept offers flexibility in tailoring different acceleration regimes and may enable coherent synchrotron radiation emission [33]. Within the framework of the NanoAc collaboration, we are also investigating potential applications, including single-shot MeV ultrafast electron diffraction, a novel mechanism for THz radiation imaging, and the development of a compact radiation source for radiotherapy. While the reported bunch charge and brightness are encouraging, the extracted beam still exhibits a relatively large divergence and energy spread. Reducing both is among the objectives of the ongoing optimization campaign, and a prerequisite for the most demanding of the aforementioned applications.

Acknowledgements The authors acknowledge the National Laboratory for Scientific Computing (LNCC/MCTI, Brazil) for providing access to the Santos Dumont supercomputer (Project LPA-FARMA), which contributed to the research results reported in this paper.

Funding Open Access funding provided thanks to the CRUE-CSIC agreement with Springer Nature. This work is supported by the Generalitat Valenciana under grant agreement CIDEGENT/2019/058. Alexandre Bonatto was partially supported by FAPERGS (Grant 24/2551-0001552-3). Bruno Silveira Nunes was supported by the CNPq (Grant 140941/2023-1).

Data availability This manuscript has associated data in a data repository.

Declarations

Conflict of interest The authors declare that they have no conflict of interest.

References

1. T. Tajima, J.M. Dawson, Laser electron accelerator. Phys. Rev. Lett. **43**(4), 267–270 (1979). https://doi.org/10.1103/PhysRevLett.43.267
2. P. Chen, J.J. Su, J.M. Dawson, K.L. Bane, P.B. Wilson, On energy transfer in the plasma wake field accelerator. Phys. Rev. Lett. **56**(12), 1252–1255 (1986). https://doi.org/10.1103/PhysRevLett.56.1252
3. S.P.D. Mangles, C.D. Murphy, Z. Najmudin, A.G.R. Thomas, J.L. Collier, A.E. Dangor, E.J. Divall, P.S. Foster, J.G. Gallacher, C.J. Hooker, D.A. Jaroszynski, A.J. Langley, W.B. Mori, P.A. Norreys, F.S. Tsung, R. Viskup, B.R. Walton, K. Krushelnick, Monoenergetic beams of relativistic electrons from intense laser-plasma interactions. Nature **431**, 535–538 (2004). https://doi.org/10.1038/nature02939
4. J. Faure, A. Pukhov, S. Kiselev, S. Gordienko, E. Lefebvre, J.-P. Rousseau, F. Burgy, V. Malka, A laser-plasma accelerator producing monoenergetic electron beams. Nature **431**, 541–544 (2004). https://doi.org/10.1038/nature02963
5. E. Esarey, C.B. Schroeder, W.P. Leemans, Physics of laser-driven plasma-based electron accelerators. Rev. Mod. Phys. **81**(3), 1229–1285 (2009). https://doi.org/10.1103/revmodphys.81.1229
6. M. Litos, E. Adli, W. An, C.I. Clarke, C.E. Clayton, S. Corde, J.P. Delahaye, R.J. England, A.S. Fisher, J. Frederico, S. Gessner, S.Z. Green, M.J. Hogan, C. Joshi, W. Lu, K.A. Marsh, W.B. Mori, P. Muggli, N. Vafaei-Najafabadi, D. Walz, G. White, Z. Wu, V. Yakimenko, G. Yocky, High-efficiency acceleration of an electron beam in a plasma wakefield accelerator. Nature **515**, 92 (2014). https://doi.org/10.1038/nature13882
7. E. Adli, A. Ahuja, O. Apsimon, R. Apsimon, A.-M. Bachmann, D. Barrientos, F. Batsch, J. Bauche, V.K. Berglyd Olsen, M. Bernardini, T. Bohl, C. Bracco, F. Braunmüller, G. Burt, B. Buttenschön, A. Caldwell, M. Cascella, J. Chappell, E. Chevallay, M. Chung, D. Cooke, H. Damerau, L. Deacon, L.H. Deubner, A. Dexter, S. Doebert, J. Farmer, V.N. Fedosseev, R. Fiorito, R.A. Fonseca, F. Friebel, L. Garolfi, S. Gessner, I. Gorgisyan, A.A. Gorn, E. Granados, O. Grulke, E. Gschwendtner, J. Hansen, A. Helm, J.R. Henderson, M. Hüther, M. Ibison, L. Jensen, S. Jolly, F. Keeble, S.-Y. Kim, F. Kraus, Y. Li, S. Liu, N. Lopes, K.V. Lotov, L. Maricalva Brun, M. Martyanov, S. Mazzoni, D. Medina Godoy, V.A. Minakov, J. Mitchell, J.C. Molendijk, J.T. Moody, M. Moreira, P. Muggli, E. Öz, C. Pasquino, A. Pardons, F. Peña Asmus, K. Pepitone, A. Perera, A. Petrenko, S. Pitman, A. Pukhov, S. Rey, K. Rieger, H. Ruhl, J.S. Schmidt, I.A. Shalimova, P. Sherwood, L.O. Silva, L. Soby, A.P. Sosedkin, R. Speroni, R.I. Spitsyn, P.V. Tuev, M. Turner, F. Velotti, L. Verra, V.A. Verzilov, J. Vieira, C.P. Welsch, B. Williamson, M. Wing, B. Woolley, G. Xia, Acceleration of electrons in the plasma wakefield of a proton bunch. Nature **561**, 363–367 (2018). https://doi.org/10.1038/s41586-018-0485-4
8. C.A. Lindstrøm, S. Corde, R. D'Arcy, S. Gessner, M. Gilljohann, M.J. Hogan, J. Osterhoff. Beam-driven plasma-wakefield acceleration. arXiv (2025). https://doi.org/10.48550/ARXIV.2504.05558. https://arxiv.org/abs/2504.05558
9. L. Labate, D. Palla, D. Panetta, F. Avella, F. Baffigi, F. Brandi, F. Di Martino, L. Fulgentini, A. Giulietti, P. Köster, D. Terzani, P. Tomassini, C. Traino, L.A. Gizzi, Toward an effective use of laser-driven very high energy electrons for radiotherapy: feasibility assessment of multi-field and intensity modulation irradiation schemes. Sci. Rep. **10**, 17307 (2020). https://doi.org/10.1038/s41598-020-74256-w
10. R.W. Assmann, M.K. Weikum, T. Akhter, D. Alesini, A.S. Alexandrova, M.P. Anania, N.E. Andreev, I. Andriyash, M. Artioli, A. Aschikhin, T. Audet, A. Bacci, I.F. Barna, S. Bartocci, A. Bayramian, A. Beaton, A. Beck, M. Bellaveglia, A. Beluze, A. Bernhard, A. Biagioni, S. Bielawski, F.G. Bisesto, A. Bonatto, L. Boulton, F. Brandi, R. Brinkmann, F. Briquez, F. Brottier, E. Bründermann, M. Büscher, B. Buonomo, M.H. Bussmann, G. Bussolino, P. Campana, S. Cantarella, K. Cassou, A. Chancé, M. Chen, E. Chiadroni, A. Cianchi, F. Cioeta, J.A. Clarke, J.M. Cole, G. Costa, M.-E. Couprie, J. Cowley, M. Croia, B. Cros, P.A. Crump, R. D'Arcy, G. Dattoli, A. Del Dotto, N. Delerue, M. Del Franco, P. Delinikolas, S. De Nicola, J.M. Dias, D. Di Giovenale, M. Diomede, E. Di Pasquale, G. Di Pirro, G. Di Raddo, U. Dorda, A.C. Erlandson, K. Ertel, A. Esposito, F. Falcoz, A. Falone, R. Fedele, A. Ferran Pousa, M. Ferrario, F. Filippi, J. Fils, G. Fiore, R. Fiorito, R.A. Fonseca, G. Franzini, M. Galimberti, A. Gallo, T.C. Galvin, A. Ghaith, A. Ghigo, D. Giove, A. Giribono, L.A. Gizzi, F.J. Grüner, A.F. Habib, C. Haefner, T. Heinemann, A. Helm, B. Hidding, B.J. Holzer, S.M. Hooker, T. Hosokai, M. Hübner, M. Ibison, S. Incremona, A. Irman, F. Iungo, F.J. Jafarinia, O. Jakobsson, D.A. Jaroszynski, S. Jaster-Merz, C. Joshi, M. Kaluza, M. Kando, O.S. Karger, S. Karsch, E. Khazanov, D. Khikhlukha, M. Kirchen, G. Kirwan, C. Kitégi, A. Knetsch, D. Kocon, P. Koester, O.S. Kononenko, G. Korn, I. Kostyukov, K.O. Kruchinin, L. Labate, C. Le Blanc, C. Lechner, P. Lee, W. Leemans, A. Lehrach, X. Li, Y. Li, V. Libov, A. Lifschitz, C.A. Lindstrøm, V. Litvinenko, W. Lu, O. Lundh, A.R. Maier, V. Malka, G.G. Manahan, S.P.D. Mangles, A. Marcelli, B. Marchetti, O. Marcouillé, A. Marocchino, F. Marteau, A. Ossa, J.L. Martins, P.D. Mason, F. Massimo, F. Mathieu, G. Maynard, Z. Mazzotta, S. Mironov, A.Y. Molodozhentsev, S. Morante, A. Mosnier, A. Mostacci, A.-S. Müller, C.D. Murphy, Z. Najmudin, P.A.P. Nghiem, F. Nguyen, P. Niknejadi, A. Nutter, J. Osterhoff, D. Oumbarek Espinos, J.-L. Paillard, D.N. Papadopoulos, B. Patrizi, R. Pattathil, L. Pellegrino, A. Petralia, V. Petrillo, L. Piersanti, M.A. Pocsai, K. Poder, R. Pompili, L. Pribyl, D. Pugacheva, B.A. Reagan, J. Resta-Lopez, R. Ricci, S. Romeo, M. Rossetti Conti, A.R. Rossi, R. Rossmanith, U. Rotundo, E. Roussel, L. Sabbatini, P. Santangelo, G. Sarri, L. Schaper, P. Scherkl, U. Schramm, C.B. Schroeder, J. Scifo, L. Serafini, G. Sharma, Z.M. Sheng, V. Shpakov, C.W. Siders, L.O. Silva, T. Silva, C. Simon, C. Simon-Boisson, U. Sinha, E. Sistrunk, A. Specka, T.M. Spinka, A. Stecchi, A. Stella, F. Stellato, M.J.V. Streeter, A. Sutherland, E.N. Svystun, D. Symes, C. Szwaj, G.E. Tauscher, D. Terzani, G. Toci, P. Tomassini, R. Torres, D. Ullmann, C. Vaccarezza, M. Valléau, M. Vannini, A. Vannozzi, S. Vescovi, J.M. Vieira, F. Villa, C.-G. Wahlström, R. Walczak, P.A. Walker, K. Wang, A. Welsch, C.P. Welsch, S.M. Weng, S.M. Wiggins, J. Wolfenden, G. Xia, M. Yabashi, H. Zhang, Y. Zhao, J. Zhu, A. Zigler, Eupraxia conceptual design report. Eur. Phys. J. Special Topics **229**(24), 3675–4284 (2020). https://doi.org/10.1140/epjst/e2020-000127-8
11. C.B. Schroeder, E. Esarey, C.G.R. Geddes, C. Benedetti, W.P. Leemans, Physics considerations for laser-plasma linear colliders. Phys. Rev. Spec. Top. Accel Beams **13**, 101301 (2010). https://doi.org/10.1103/physrevstab.13.101301

12. T. Tajima, M. Cavenago, Crystal x-ray accelerator. Phys. Rev. Lett. **59**(13), 1440–1443 (1987). https://doi.org/10.1103/PhysRevLett.59.1440
13. P. Chen, R.J. Noble. A solid state accelerator. In: Advanced Accelerator Concepts. AIP Conference Proceedings, vol. 156, pp. 222–227. AIP, Madison, WI, USA (1987). https://doi.org/10.1063/1.36458
14. X. Zhang, T. Tajima, D. Farinella, Y. Shin, G. Mourou, J. Wheeler, P. Taborek, P. Chen, F. Dollar, B. Shen, Particle-in-cell simulation of x-ray wakefield acceleration and betatron radiation in nanotubes. Phys. Rev. Accel. Beams **19**(10), 101004 (2016). https://doi.org/10.1103/PhysRevAccelBeams.19.101004
15. D.S. Bondar, V.I. Maslov, I.N. Onishchenko, Investigation of the way of phase synchronization of a self-injected bunch and an accelerating wakefield in solid-state plasma. Photonics **9**(3), 174 (2022). https://doi.org/10.3390/photonics9030174
16. P. Kumar Singh, I. Chakraborty, G. Chatterjee, A. Adak, A.D. Lad, P. Brijesh, P. Ayyub, G. Kumar, R. Kumar, Enhanced transport of relativistic electrons through nanochannels. Phys. Rev. ST-AB **16**, 063401 (2013). https://doi.org/10.2203/PhysRevSTAB.16.063401
17. S. Jiang, A.G. Krygier, D.W. Schumacher, K.U. Akli, R.R. Freeman, Effects of front-surface target structures on properties of relativistic laser-plasma electrons. Phys. Rev. E **89**, 013106 (2014). https://doi.org/10.1103/PhysRevE.89.013106
18. S. Jiang, L.L. Ji, H. Audesirk, K.M. George, J. Snyder, A.G. Krygier, P. Poole, C. Willis, R. Daskalova, E. Chowdhury, N.S. Lewis, D.W. Schumacher, A. Pukhov, R.R. Freeman, K.U. Akli, Microengineering laser plasma interactions at relativistic intensities. Phys. Rev. Lett. **116**, 085002 (2016). https://doi.org/10.1103/PhysRevLett.116.085002
19. S. Mondal, I. Chakraborty, S. Admad, D. Carvalho, P. Singh, A.D. Lad, V. Narayanan, P. Ayyub, G. Ravindra Kumar, Highly enhanced hard x-ray emission from oriented metal nanorod arrays excited by intense femtosecond laser pulses. Phys. Rev. B **83**, 035408 (2011). https://doi.org/10.1103/PhyRevB.83.035408
20. G. Cristoforetti, P. Londrillo, P.K. Singh, F. Baffigi, G. D'Arrigo, A.D. Lad, R.G. Milazzo, A. Adak, M. Shaikh, D. Sarkar, G. Chatterjee, J. Jha, M. Krishnamurthy, G.R. Kumar, L.A. Gizzi, Transition from coherent to stochastic electron heating in ultrashort relativistic laser interaction with structured targets. Sci. Rep. **7**, 1479 (2017). https://doi.org/10.1038/s41598-017-01677-5
21. R. Xie, L.H. Cao, Y. Chao, Y. Jiang, Z.J. Liu, C.Y. Zheng, X.T. He, Improvement of laser absorption and control of particle acceleration by subwavelength nanowire target. Phys. Plasmas **27**, 123108 (2020). https://doi.org/10.1063/5.0022144
22. E. Eftekhari-Zadeh, M.S. Blümcke, Z. Samsonova, R. Loetzsch, I. Uschmann, M. Zapf, C. Ronning, O.N. Rosmej, D. Kartashov, C. Spielmann, Laser energy absorption and x-ray generation in nanowire arrays irradiated by relativistically intense ultra-high contrast femtosecond laser pulses. Phys. Plasmas **29**, 013301 (2022). https://doi.org/10.1063/5.0064364
23. J.J. Rocca, M.G. Capeluto, R.C. Hollinger, S. Wang, Y. Wang, G.R. Kumar, A.D. Lad, A. Pukhov, V.N. Shlyaptsev, Ultra-intense femtosecond laser interaction with aligned nannostructures. Optica **11**, 437 (2024). https://doi.org/10.1364/OPTICA.510542
24. Margarone D, Klimo1 O, Kim IJ, Prokůpek J, Limpouch J,Jeong TM, Mocek T, Pšikal J, Kim HT, Proška J, Nam KH, Štolcová L, Choi, Lee SK, Sung JH, Yu TJ, Korn G, Laser-driven proton acceleration enhancement by nanostructured foils. Phys. Rev. Lett. **109**, 234801 (2012). https://doi.org/10.1103/PhysReLett.109.234801
25. J. Resta-López, A. Alexandrova, V. Rodin, Y. Wei, C.R. Welsch, I, Y., G. Xia, Y. Zhao, Study of ultra-high gradient acceleration in carbon nanotube arrays. In: Proceedings 9th International Particle Accelerator Conference (IPAC'18), Vancouver, BC, Canada, April 29-May 4, 2018, pp. 599–602 (2018). https://doi.org/10.18429/JACoW-IPAC2018-TUXGBE2
26. A. Bonatto, G. Xia, O. Apsimon, C. Bontoiu, E. Kukstas, V. Rodin, M. Yadav, C.P. Welsch, J. Resta-López, Exploring ultra-high-intensity wakefields in carbon nanotube arrays: an effective plasma-density approach. Phys. Plasmas **30**, 033105 (2023). https://doi.org/10.1063/5.0134960
27. C. Bonţoiu, A. Bonatto, O. Apsimon, L. Bandiera, G. Cavoto, I. Drebot, G. Gatti, J. Giner-Navarro, B. Lei, P. Martín-Luna, I. Rago, J. Rodríguez Pérez, B.S. Nunes, A. Sytov, C. Valagiannopoulos, C.P. Welsch, G. Xia, J. Zhang, J. Resta-López, Numerical study of self-injected electron acceleration in cnt structured targets driven by an 800 nm laser. Sci. Rep. **15**, 45323 (2025). https://doi.org/10.1038/s41598-025-29386-4
28. B. Galante, G.A. Tranquille, M. Himmerlich, C.P. Welsch, J. Resta-López, Stability and lifetime study of carbon nanotubes as cold electron field emitters for electron cooling in the cern extra low energy antiproton ring. Phys. Rev. Accel. Beams **24**, 113401 (2021). https://doi.org/10.1103/PhysRevAccelBeams.24.113401
29. G. Aliana-Cervera, D. Mattia, C. Pasquino, R. Veness, A.J.G. Lunt, Carbon nanotube wires for accelerator applications. Mater. Des. **258**, 114606 (2025). https://doi.org/10.1016/j.matdes.2025.114606
30. C. Bonţoiu, O. Apsimon, E. Kukstas, V. Rodin, M. Yadav, C.P. Welsch, J. Resta-López, A. Bonatto, G. Xia, Tev/m catapult acceleration of electrons in graphene layers. Sci. Rep. **13**, 1330 (2023). https://doi.org/10.1038/s41598-023-28617-w
31. B. Lei, H. Zhang, C. Bonţoiu, A. Bonatto, J. Resta-López, G. Xia, B. Qiao, C. Welsch, 100 s tev/m-level particle accelerators driven by high-density electron beams in micro structured carbon nanotube forest channel. New J. Phys. **27**, 084301 (2025). https://doi.org/10.1088/1367-2630/adf87d
32. B. Lei, H. Zhang, C. Bonţoiu, A. Bonatto, P. Martín-Luna, B. Liu, J. Resta López, G. Xia, C.P. Welsch, Leaky surface plasmon-based wakefield acceleration in nanostructured carbon nanotubes. Plasma Phys. Control. Fusion **67**, 065036 (2025). https://doi.org/10.1088/1361-6587/ade00a
33. B. Lei, H. Zhang, D. Seipt, A. Bonatto, B. Qiao, J. Resta-López, G. Xia, Welsch: coherent synchrotron radiation by excitation of surface plasmon polariton on near-critical solid microtube surface. Phys. Rev. Lett. **135**, 205001 (2025). https://doi.org/10.1103/cnym-16hc
34. Application of Nanostructures in the Field of Accelerator Physics (NanoAc 2022). Workshop. International Workshop, Indico IFIC, Valencia, Spain (2022). https://indico.ific.uv.es/event/6833/
35. 2nd Workshop on Applications of Nanostructures in the Field of Accelerator Physics (NanoAc 2024). Workshop. International Workshop, ICMUV Forum, Valencia, Spain (2024). https://forum.icmuv.uv.es/event/3/
36. 3rd NanoAc Workshop on Applications of Nanostructures in the Field of Accelerator Physics (NanoAc 2025). Workshop. International Workshop, University of Liverpool, UK (2025). https://indico.ph.liv.ac.uk/event/2027/
37. J.-L. Vay, M. Acciarri, A. Almgren, L.D. Amorim, I. Andriyash, J.R. Angus, T. Antoun, D. Belkin, D. Bizzozero, A. Blelly, S.E. Clark, E. Dammak, L. Fedeli, A. Formenti, M. Garten, L. Ge, L. Giacomel, K. Gott, L. Giacomel, R.E. Groenewald, D. Grote, J. Gu, C. Harrison, M. Haseeb, A. Huebl, R. Jambunathan, I. Kara-Mostefa, H. Klion, P. Kumar, R. Lehe, B. Loring, T. Marks, P. Miller, A. Myers, J. Pech, E. Rheaume, G. Richardson, E. Rheaume, M.E. Rowan, R.T. Sandberg, P. Scherpelz, A. Sinn, O. Shapoval, D. Terzani, M. Thévenet, K. Weichman, E. Yang, N. Zaim, W. Zhang, Y. Zhao, K.Z. Zhu, E. Zoni, WarpX: an advanced Particle-In-Cell code. Zenodo (2018). https://doi.org/10.5281/zenodo.4571577
38. A.A. Sahai, Excitation of a nonlinear plasma ion wake by intense energy sources with applications to the crunch-in regime. Phys. Rev. Accel. Beams **20**(8), 081004 (2017). https://doi.org/10.1103/PhysRevAccelBeams.20.081004
39. A.A. Sahai, T. Tajima, P. Taborek, V.D. Shiltsev, Solid-state tube wakefield accelerator using surface waves in crystals. Int. J. Mod. Phys. A **34**(34), 1943009 (2019). https://doi.org/10.1142/S0217751X19430097
40. R.P. Shanks, M.P. Anania, E. Brunetti, S. Cipiccia, B. Ersfeld, J.G. Gallacher, R.C. Issac, M.R. Islam, G. Vieux, G.H. Welsh, S.M. Wiggins, D.A. Jaroszynski. Pepper-pot emittance measurement of laser-plasma wakefield accelerated electrons. In: Jaroszynski, D.A., Rousse, A. (eds.) Harnessing Relativistic Plasma Waves as Novel Radiation Sources From Terahertz to X-Rays and Beyond, p. 735907. SPIE – The International Society for Optical Engineering, Prague, Czech Republic (2009). https://doi.org/10.1117/12.820706

41. Y. Wu, D. Han, B. Zhu, K. Dong, F. Tan, Y. Gu, A new method to calculate the beam charge for an integrating current transformer. Rev. Sci. Instrum. **83**(9), 093302 (2012). https://doi.org/10.1063/1.4750072
42. J.M. Khosrofian, B.A. Garetz, Measurement of a gaussian laser beam diameter through the direct inversion of knife-edge data. Appl. Opt. **22**(21), 3406–3410 (1983). https://doi.org/10.1364/AO.22.003406
43. A. Thess, R. Lee, P. Nikolaev, H. Dai, P. Petit, J. Robert, C. Xu, Y.H. Lee, S.G. Kim, A.G. Rinzler, D.T. Colbert, G.E. Scuseria, D. Tománek, J.E. Fischer, R.E. Smalley, Crystalline ropes of metallic carbon nanotubes. Science **273**(5274), 483–487 (1996). https://doi.org/10.1126/science.273.5274.483
44. C.H. See, A.T. Harris, A review of carbon nanotube synthesis via fluidized-bed chemical vapor deposition. Ind. Eng. Chem. Res. **46**, 997–1012 (2007). https://doi.org/10.1021/ie060955b
45. F. Sarasini, J. Tirillò, M. Lilli, M.P. Bracciale, P.E. Vullum, F. Berto, G. De Bellis, A. Tamburrano, G. Cavoto, F. Pandolfi, I. Rago, Highly aligned growth of carbon nanotube forests with in-situ catalyst generation: a route to multifunctional basalt fibres. Compos. B Eng. **243**, 110136 (2022). https://doi.org/10.1016/j.compositesb.2022.110136
46. E. Schifano, G. Cavoto, F. Pandolfi, G. Pettinari, A. Apponi, A. Ruocco, D. Uccelletti, I. Rago, Plasma-etched vertically aligned CNTs with enhanced antibacterial power. Nanomaterials **13**, 1081 (2023). https://doi.org/10.3390/nano13061081
47. R.P. Yadav, I. Rago, F. Pandolfi, C. Mariani, A. Ruocco, S. Tayyab, A. Apponi, G. Cavoto, Evaluation of vertical alignment in carbon nanotubes: a quantitative approach. Nucl. Instrum. Methods Phys. Res. A **1060**, 169081 (2024). https://doi.org/10.1016/j.nima.2024.169081
48. K. Wang, F. Wang, Q. Jiang, P. Zhu, K. Leu, R. Zhang, Controlled synthesis, properties, and applications of ultralong carbon nanotubes. Nanoscale Adv. **6**, 4504 (2024). https://doi.org/10.1039/d4na00437j
49. Technology Innovation Through Advanced Nanostructures (TITAN), Dipartamento di Fisica, Sapienza Università di Roma. https://www.phys.uniroma1.it/it/technology-innovation-through-advanced-nanostructures-titan
50. Center of Pulsed Lasers (CLPU). https://www.clpu.es/eu/laser-vega-pw